

Surface Oxidation of Tin Chalcogenide Nanocrystals Revealed by ^{119}Sn –Mössbauer Spectroscopy

Antoine de Kergommeaux,^{†,‡} Jérôme Faure-Vincent,[†] Adam Pron,^{†,||} Rémi de Bettignies,[‡] Bernard Malaman,[§] and Peter Reiss*,[†]

[†]CEA Grenoble, INAC, UMR 5819 SPrAM (CEA/CNRS/UJF-Grenoble 1), Laboratoire d'Electronique Moléculaire, Organique et Hybride, 17 rue des Martyrs, 38054 Grenoble cedex 9, France

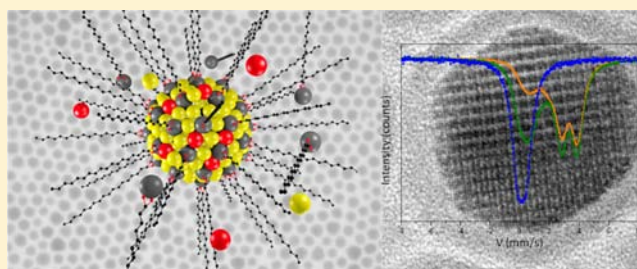
[‡]INES, CEA-DRT/LITEN/DTS/LMPV, Institut National de l'Energie Solaire, Le Bourget du Lac, France

[§]Institut Jean Lamour, Université de Lorraine, UMR 7198, B.P. 70239, 54506 Vandoeuvre-les-Nancy Cedex, France

^{||}Faculty of Chemistry, Warsaw University of Technology, Noakowskiego 3 00664 Warszawa, Poland

Supporting Information

ABSTRACT: Narrow band gap tin(II) chalcogenide (SnS, SnSe, SnTe) nanocrystals are of high interest for optoelectronic applications such as thin film solar cells or photo-detectors. However, charge transfer and charge transport processes strongly depend on nanocrystals' surface quality. Using ^{119}Sn –Mössbauer spectroscopy, which is the most sensitive tool for probing the Sn oxidation state, we show that SnS nanocrystals exhibit a $\text{Sn}^{(\text{IV})}/\text{Sn}^{(\text{II})}$ ratio of around 20:80 before and 40:60 after five minutes exposure to air. Regardless of the tin or sulfur precursors used, similar results are obtained using six different synthesis protocols. The $\text{Sn}^{(\text{IV})}$ content before air exposure arises from surface related SnS_2 and Sn_2S_3 species as well as from surface Sn atoms bound to oleic acid ligands. The increase of the $\text{Sn}^{(\text{IV})}$ content upon air exposure results from surface oxidation. Full oxidation of the SnS nanocrystals without size change is achieved by annealing at 500 °C in air. With the goal to prevent surface oxidation, SnS nanocrystals are capped with a cadmium–phosphonate complex. A broad photoluminescence signal centered at 600 nm indicates successful capping, which however does not reduce the air sensitivity. Finally we demonstrate that SnSe nanocrystals exhibit a very similar behavior with a $\text{Sn}^{(\text{IV})}/\text{Sn}^{(\text{II})}$ ratio of 43:57 after air exposure. In the case of SnTe nanocrystals, the ratio of 55:45 is evidence of a more pronounced tendency for oxidation. These results demonstrate that prior to their use in optoelectronics further surface engineering of tin chalcogenide nanocrystals is required, which otherwise have to be stored and processed under inert atmosphere.



INTRODUCTION

For many types of semiconductor nanocrystals (NCs), the precise control of size, shape, and composition has been achieved by optimization of their chemical synthesis methods. Their size-dependent physical properties and solution processability make them promising building blocks for a number of electronic and optoelectronic devices,¹ such as field-effect transistors^{2–7} or solar cells.^{8–16} On the other hand, the materials used in this domain of electronics are almost exclusively based on lead or cadmium chalcogenides, apart from few exceptions.^{17–20} Given the risk of these toxic elements containing materials for human health and environment, it is not surprising that nowadays significant research efforts are undertaken to develop NCs of alternative, environmentally more friendly materials. For applications relying on the efficient harvesting of solar light, narrow band gap semiconductors ($E_g \approx 1.5$ eV or lower) are of particular interest. Beside copper or iron chalcogenide NCs^{21–25} tin chalcogenide (SnX, X = S, Se, Te) NCs could be very interesting candidates for cost efficient photovoltaic applications. Several protocols for the

synthesis of SnX NCs have been reported,^{26–29} but their successful integration into (opto-)electronic devices has not yet been achieved.

For all applications of NCs, their surface properties are of crucial importance. In particular, surface ligands play an important role in charge transfer, charge carriers transport, and electronic coupling between NCs. In addition to traditional organic surfactants, fully inorganic surface stabilization by metal chalcogenide complexes or simply by ions has recently been reported, resulting in improved charge carrier mobilities.^{30–35} However, preparation and processing of small size SnX-type NCs is a delicate matter due to the fact that these compounds, even in their bulk state, show a rather low resistance against oxidation. In NCs, this resistance is even lower as a consequence of the large ratio of surface atoms to bulk ones. Surface oxidation has a disastrous effect on essentially all physicochemical properties of NCs and can be considered as a

Received: April 6, 2012

Published: June 13, 2012

key limiting factor for their electronic applications. Oxidation phenomena cause charges trapping inside the NCs and reduce electrical transport. While surface oxidation has been observed for tin NCs,³⁶ this phenomenon has not yet been investigated in the case of SnX NCs; the study of the oxidation mechanism and the determination of the tin oxidation state in SnX NCs' bulk volume and surfacial atoms are challenging tasks. On the other hand, the understanding of these factors is critical for controlling and avoiding oxidation phenomena and for the future technological use of SnX NCs. To give an example, partially oxidized NCs are electronically inert, whereas fully crystallized oxides are finding applications in gas sensors.^{37–43}

Here we explore six different protocols for the synthesis of SnS NCs and investigate the influence of the reaction parameters on their size, shape, composition, crystal structure and band gap using powder X-ray diffraction (XRD), energy dispersive X-ray spectroscopy (EDS), transmission electron microscopy (TEM), scanning transmission electron microscopy (STEM), and UV–vis/near-infrared absorption spectroscopy. Only for one synthesis protocol, an amorphous shell on the SnS NC surface was observed with HRTEM. However, ¹¹⁹Sn Mössbauer spectroscopy, which is the most accurate tool for the determination of the tin atoms oxidation state, also in extremely thin amorphous layers of a subnanometric thickness, reveals that a substantial amount of Sn^(IV) is present in all samples. ¹¹⁹Sn Mössbauer spectroscopy thus demonstrates the strong tendency of SnS NCs for surface oxidation regardless of the used synthesis protocol. A similar behavior is observed for SnSe NCs, while SnTe NCs show an even more pronounced sensitivity toward oxidation.

EXPERIMENTAL SECTION

Materials. Tin(II) chloride (>99.995%, anhydrous), thioacetamide (>99.0%), bis[bis(trimethylsilyl)amino] tin(II), sulfur (>99.998%), selenium (99.54%), tellurium (99.95%), oleic acid (70%), trioctylphosphine (90%), octadecene (90%) and anhydrous solvents were purchased from Sigma-Aldrich. Oleylamine (70%) was obtained from Fluka. All compounds were stored and used in a glovebox.

SnS NCs' Synthesis. All syntheses were carried out using a vacuum/argon Schlenk line and a glovebox avoiding any exposure of the chemicals to air and moisture.

Protocol A. Anhydrous tin chloride powder (SnCl₂, 380 mg, 2 mmol) was loaded into a 50 mL three-neck flask with octadecene (ODE, 5 mL, 15.6 mmol), trioctylphosphine (TOP, 3 mL, 6.7 mmol) and oleic acid (OA, 4.5 mL, 14.2 mmol) and degassed under primary vacuum during 1 h at 60 °C. Next the temperature was increased to 100 °C and a solution containing thioacetamide (TAA, 75 mg, 1 mmol), oleylamine (OLA, 5 mL, 15.2 mmol) and trioctylphosphine (TOP, 3 mL, 6.7 mmol) was swiftly injected under vigorous stirring. The reaction was left at this temperature for 5 min to 1 h depending of the desired NC size and then quickly cooled down with help of an ice bath. A chloroform/ethanol mixture (20 mL, 1:2 vol/vol) was added to precipitate the NCs, which were collected by centrifugation at 5000 rpm for 3 min. After dispersion in 10 mL of chloroform, the NCs were purified a second time using the same precipitation method and finally dispersed in 10 mL of chloroform to form stable colloidal solutions.

Protocol B. This protocol, reported by Hickey et al.,²⁶ relies on the use of a different tin precursor, namely bis[bis(trimethylsilyl)amino]tin(II) (((TMS)₂N)₂Sn, 0.78 mL, 2 mmol) instead of tin chloride. Otherwise, all parameters were kept identical as in procedure A.

Protocol C. With the same synthesis parameters as in protocol A and B, bis[bis(trimethylsilyl)amino]tin(II) (((TMS)₂N)₂Sn, 0.78 mL, 2 mmol) was used as the tin precursor and bis(trimethylsilyl)sulfur ((TMS)₂S, 210 μL, 1 mmol) was used as sulfur precursor.

Protocol D. This procedure is adapted from Liu et al.²⁷ With the same synthesis parameters as protocol A, anhydrous tin chloride

powder (SnCl₂, 380 mg, 2 mmol) was used as tin precursor and bis(trimethylsilyl)sulfur ((TMS)₂S, 210 μL, 1 mmol) was used as sulfur precursor.

Protocol E. With the same synthesis parameters as protocol A, bis[bis(trimethylsilyl)amino]tin(II) (((TMS)₂N)₂Sn, 0.78 mL, 2 mmol) was used as tin precursor and elemental sulfur (S, 32 mg, 1 mmol) was used as sulfur precursor.

Protocol F. With the same synthesis parameters as protocol A, anhydrous tin chloride powder (SnCl₂, 380 mg, 2 mmol) was used as tin precursor and elemental sulfur (S, 32 mg, 1 mmol) was used as sulfur precursor.

Table 1 summarizes the precursors used in each protocol.

Table 1. Precursors' Repartition in the Different Synthesis Protocols

	thioacetamide	(TMS) ₂ S	S (elemental)
((TMS) ₂ N) ₂ Sn	Protocol B	Protocol C	Protocol E
SnCl ₂	Protocol A	Protocol D	Protocol F

SnSe Synthesis. SnSe NCs were synthesized following the procedure reported by Baumgardner et al.²⁸ Briefly, 1 mL of TOP-Se stock solution (79 mg/1 mmol of Se in 1 mL of TOP) was loaded into a 50 mL three-neck flask containing OLA (5 mL, 15.2 mmol) and degassed for 1 h at 100 °C. The temperature was then increased to 130 °C and a solution of bis[bis(trimethylsilyl)amino]tin(II) (((TMS)₂N)₂Sn, 0.16 mL, 0.4 mmol) in 2 mL of ODE was swiftly injected under vigorous stirring. After 1.5 min, 3 mL of OA were injected and the solution was cooled down with an ice bath. The solution was left stirring at room temperature for 15 min. A chloroform/ethanol mixture (20 mL, 1:2 vol/vol) was added and the precipitated NCs were collected by centrifugation at 9000 rpm for 2 min. After dispersion in chloroform, the purification by precipitation was repeated and the NCs were finally dispersed in chloroform to form stable colloidal solutions.

SnTe Synthesis. SnTe NCs were synthesized according to the protocol described by Kovalenko et al.²⁹ In brief, a 0.78 M TOP-Te stock solution was prepared by dissolving 995 mg of elemental Te in 10 mL of TOP at 300 °C. The solution was orange at high temperature and turned greenish yellow at room temperature. One milliliter of TOP-Te stock solution was injected into a 50 mL three-neck flask containing 5 mL of OLA. The mixture was degassed under primary vacuum at 100 °C for 1 h. The temperature was then increased to 130 °C and a solution of bis[bis(trimethylsilyl)amino]tin(II) (((TMS)₂N)₂Sn, 0.16 mL, 0.4 mmol) in 2 mL of ODE was swiftly injected under vigorous stirring. After 1.5 min, 3 mL of OA were added and the mixture was cooled down with an ice bath. It was left stirring at room temperature for 15 min. Purification of the NCs was carried out in the same way as described for SnSe.

Cd-complex Surface Passivation of SnS NCs. The surface passivation procedure using Cd–phosphonate complexes as described by Tang et al. was applied.¹³ Cadmium chloride (CdCl₂, 103 mg, 0.8 mmol), tetradecylphosphonic acid (TDPA, 40 mg) and oleylamine (OLA, 4 mL) were degassed under primary vacuum at 100 °C for 1 h. To this mixture was added 8 mL of a 20 mg/mL dispersion of SnS NCs in chloroform followed by 16 mL of toluene. The mixture was then heated to 60 °C for 5 min and cooled down to room temperature. Purification of the NCs was carried out in the same way as described for SnSe.

SnS NCs' Oxidation. To fully oxidize SnS NCs (yielding SnO₂ NCs), we heated them in an oven under air at 500 °C for 10 h. The black SnS NCs turned yellow indicating the formation of SnO₂.

Characterization Methods. Transmission electron microscopy (TEM) images of the obtained NCs have been recorded using a JEOL 4000EX High Resolution Transmission Electron Microscope (HRTEM) operated at 400 kV. Scanning Electron Microscopy (SEM) and Scanning Transmission Electron Microscopy (STEM) images were acquired with a ZEISS Ultra 55+ Electron Microscope. For TEM and STEM, the NCs were drop-cast on carbon coated

copper grids (Ted Pella) and dried under vacuum. Powder X-ray diffraction has been carried out with a PHILIPS X'Pert powder diffractometer with a cobalt cathode ($\lambda = 1.789 \text{ \AA}$) operating at 40 kV and 40 mA. For sample preparation, the concentrated colloidal solution was drop-cast onto a disoriented silicon substrate. UV–visible absorption spectra were measured with a HEWLETT PACKARD 8452A diode array spectrophotometer using quartz cuvettes. Photoluminescence (PL) spectra were recorded on a Hitachi F-4500 spectrofluorometer. The ^{119}Sn Mössbauer measurements were carried out using a constant acceleration spectrometer in standard transmission geometry. Spectra were recorded at 5 K thanks to a liquid helium cryostat. The velocity scale was calibrated with a $^{57}\text{CoRh}$ source (25 mCi) and a metallic iron foil at room temperature. We used a $\text{Ba}^{119}\text{mSnO}_3$ source (10 mCi) kept at room temperature which also served as the reference for the isomer shifts. A polycrystalline absorber with natural abundance of ^{119}Sn isotope and thickness of $\sim 15 \text{ mg cm}^{-2}$ was used. A palladium foil of 0.5 mm thickness was used as a critical absorber for tin X-rays. The Mössbauer spectra were fitted with a least-squares method assuming Lorentzian peaks (cf. Supporting Information). The error on all of the ^{119}Sn Mössbauer spectra was $\pm 0.1 \text{ mm s}^{-1}$.

RESULTS AND DISCUSSION

Synthesis of SnS NCs. With the goal to evaluate in more detail the influence of reaction parameters on the properties of SnS NCs, we investigated a number of synthesis methods combining two different tin precursors with three different sulfur precursors. Two of these methods have been reported in literature:^{26,27} the first one, called here *protocol B*,²⁶ is based on $((\text{TMS})_2\text{N})_2\text{Sn}$, already used in earlier works^{28,29} combined with thioacetamide as sulfur precursor. The second one, referred to as *protocol D*,²⁷ consists of reacting tin(II)chloride with $(\text{TMS})_2\text{S}$, which is known to be a highly reactive sulfur precursor. We further investigated the use of four novel protocols (cf. Table 1) applying elemental sulfur as an additional sulfur source. All protocols yielded colloidal solutions of SnS NCs except for *protocol C*, which combines $((\text{TMS})_2\text{N})_2\text{Sn}$ and $(\text{TMS})_2\text{S}$. The particles prepared using this protocol precipitate, even at a comparably low reaction temperature of 100 °C. A synthesis carried out at 60 °C gave noncrystalline particles showing a high degree of aggregation (cf. Supporting Information).

The UV–vis–NIR absorption spectra of the obtained NCs (Figure 1a) show that the onset of the absorbance increase is located at around 700 nm for all samples, except for the larger particles obtained using *protocol C* ($\sim 900 \text{ nm}$). On the basis of the direct band gap value of bulk SnS (1.3 eV), an absorption onset of approximately 950 nm would be expected in the

absence of quantum confinement effects. Except for Hall effect measurements,⁴⁵ not many data concerning the electronic properties of SnS NCs are available, rendering the estimation of the Bohr exciton radius difficult. So far, no correlation between size and band gap has been reported for this material. The powder X-ray diffraction data of the SnS NCs (Figure 1b) indicate that all protocols yield the same crystal structure, with peak width variations originating from different NCs' sizes. Bulk SnS predominantly crystallizes in the orthorhombic crystal system (space group $Pnma$) while the diffractograms obtained here correspond to α -SnS in the orthorhombic space group $Pbmm$ ($a = 4.3291$, $b = 11.1923$, $c = 3.9838 \text{ \AA}$).

In contrast to the XRD data and absorption spectra, STEM and HRTEM studies (cf. Figure 2) reveal significant differences between the obtained samples. Protocols A and D, in which SnCl_2 is used as the tin precursor, yield NCs of a mean size of 13 and 7.5 nm, respectively, showing narrow size distribution. In both cases, the size can be tuned from 5 to 25 nm by controlling temperature (80–150 °C) and reaction time (5–120 min). Protocol E, based on the use of $((\text{TMS})_2\text{N})_2\text{Sn}$ and elemental sulfur, yields NCs of a mean size of 17 nm and also relatively low size dispersion, while the samples obtained with protocols B and F exhibit a broad distribution of sizes and shapes. The lattice parameters extracted from HRTEM images correspond to the (121) planes (2.6 Å), (101) planes (2.9 Å), and (021) planes (3.1 Å). In the HRTEM image shown in Figure 2a, we can clearly distinguish an approximately 5 nm thick, apparently amorphous shell surrounding the NC, which is absent in the nanoparticles prepared by other protocols. If surface oxidation phenomena were at the origin of the shell formation, the NCs should be sulfur deficient. However, Energy Dispersive X-ray spectroscopy (EDS) measurements (cf. Table 2) reveal that this is not the case; for all protocols, a Sn/S ratio close to 1:1 is obtained.

Determination of the Sn Oxidation State in the Obtained Nanocrystals. ^{119}Sn Mössbauer spectroscopy is the most adapted and precise way to characterize the different oxidation states of the tin atoms in a stannide compound. It is based on a recoilless emission and resonant absorption of γ -radiation by atomic nuclei, giving the narrowest line width and hence the highest resolution of all spectroscopic techniques. The dependence of the phenomenon on temperature and solid vibration energies is taken into account for by the elemental-specific Lamb-Mössbauer factor. Since this factor represents the probability for the recoil energy to excite lattice vibrations and to change the nucleus state, its temperature dependence is not the same for $\text{Sn}^{(0)}$, $\text{Sn}^{(\text{II})}$ and $\text{Sn}^{(\text{IV})}$, and for this reason the experiments have to be carried out at low temperature. From these measurements, several characteristic parameters can be extracted. The first crucial parameter is the difference between s-electrons density in the source and in the sample that leads to a shift of the whole spectrum, called the isomer shift (IS). The IS value is relative to the source and needs to be referred to a known reference. The second parameter is the quadrupolar splitting (EQ) which represents the energy difference between substates induced by the angular momentum quantum number. In ^{119}Sn isotopes two substates for tin(II) can be distinguished for the excited state, which give rise to two transitions. As a result a doublet appears in the spectra. While EQ gives information about the nucleus environment, the peak areas reflect the proportion of each different species in the sample ($\text{Sn}^{(0)}$, $\text{Sn}^{(\text{II})}$ or $\text{Sn}^{(\text{IV})}$).

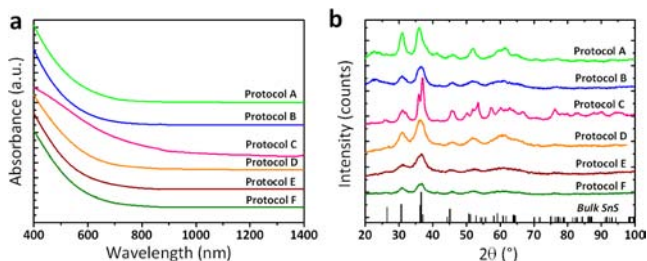


Figure 1. (a) UV–vis–NIR absorption spectra of SnS NCs in chloroform using different synthesis protocols. (b) X-ray diffractograms of the same samples measured using a cobalt source ($\lambda = 1.789 \text{ \AA}$) compared to the reference pattern of bulk SnS showing the orthorhombic space group $Pbmm$ (JCPDS #39–354).⁴⁴ The spectra have been normalized and vertically shifted for clarity.

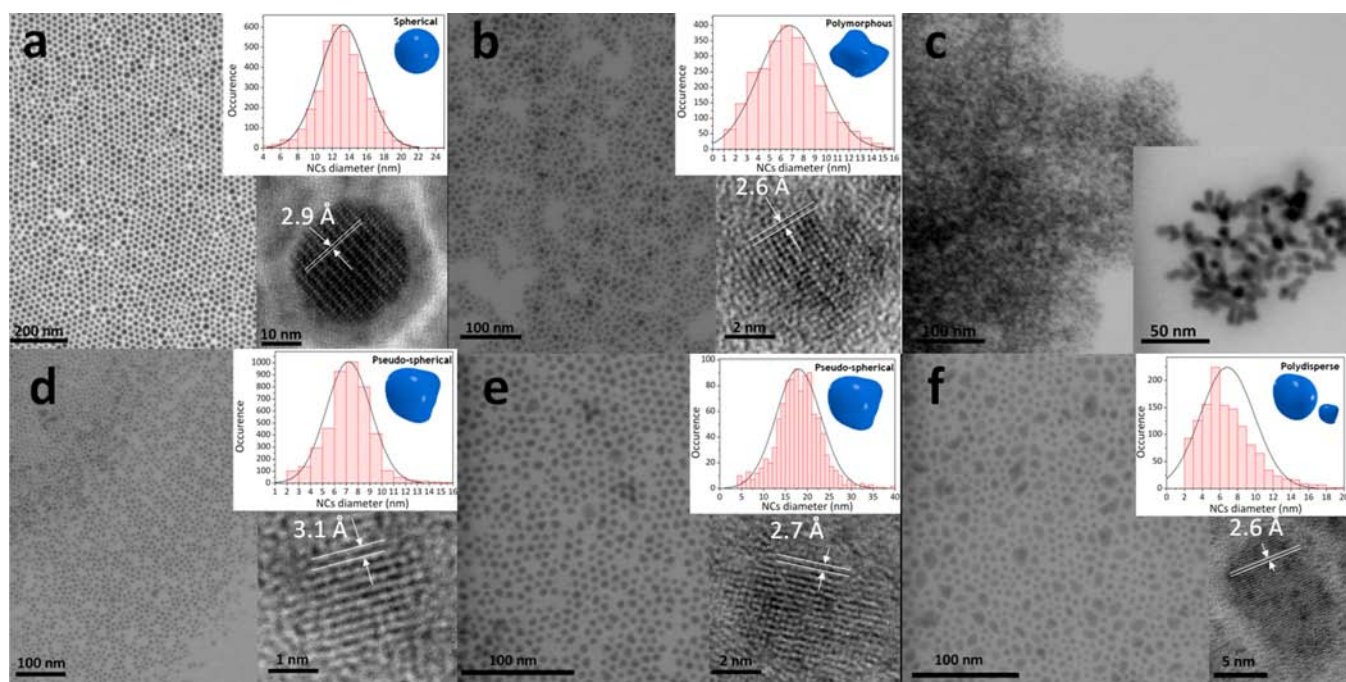


Figure 2. STEM and HRTEM images as well as size distribution of the SnS nanocrystals synthesized using (a) Protocol A, (b) Protocol B, (c) Protocol C (no HRTEM image), (d) Protocol D, (e) Protocol E, and (f) Protocol F.

Table 2. Summary of EDS Ratios, SnS NCs Size by XRD, and STEM

protocols	EDS ratio		XRD size	STEM size
	tin	sulfur		
Protocol A	46.5%	53.5%	13 nm	14 nm
Protocol B	48.6%	51.4%	7 nm	7 nm
Protocol C	45.5%	54.5%	23 nm	—
Protocol D	48.0%	52.0%	7 nm	7 nm
Protocol E	48.4%	51.6%	15 nm	17 nm
Protocol F	47.5%	52.5%	7 nm	8 nm

The Mössbauer spectra, recorded at 5 K (Figure 3), exhibit the same three peaks for all protocols.

We expected to observe a difference between the spectrum of sample A, showing a core/shell structure in HRTEM images, and the spectra of the other samples. However, all samples show a broadened peak around $0.40 \text{ mm}\cdot\text{s}^{-1}$ and a doublet centered at $\sim 3.25 \text{ mm}\cdot\text{s}^{-1}$. These IS values are in agreement with the occurrence of tin atoms in +IV and +II oxidation states, respectively. Except for protocol D which seems to yield a lower fraction of $\text{Sn}^{(\text{IV})}$ (around 15%), all protocols exhibit the same proportions of $\text{Sn}^{(\text{IV})}$ and $\text{Sn}^{(\text{II})}$, on the order of 40:60. The broadened peaks at $\sim 0.5 \text{ mm}\cdot\text{s}^{-1}$ can be attributed to $\text{Sn}^{(\text{IV})}$ compounds, namely SnO_2 , Sn_2S_3 and/or SnS_2 .^{46–49} The best fit of the experimental data could be obtained by combining all three phases (cf. Supporting Information). To give an example, a hypothetical NC composition of 60% SnS, 30% SnS_2 , 5% Sn_2S_3 and 5% SnO_2 would be in accordance with both the results from Mössbauer spectroscopy ($\text{Sn}^{(\text{IV})}/\text{Sn}^{(\text{II})} \approx 40:60$) and from EDS analysis ($\text{Sn}/\text{S} \approx 47:53$). According to the XRD data, the $\text{Sn}^{(\text{IV})}$ phases are in an amorphous state. We therefore attribute the singlet peak at $\sim 0.5 \text{ mm}\cdot\text{s}^{-1}$ to an amorphous ternary phase composed of tin, sulfur, and oxygen. The doublet centered at $\sim 3.25 \text{ mm}\cdot\text{s}^{-1}$ can be clearly attributed to SnS ,⁴⁹ in agreement with the XRD data.

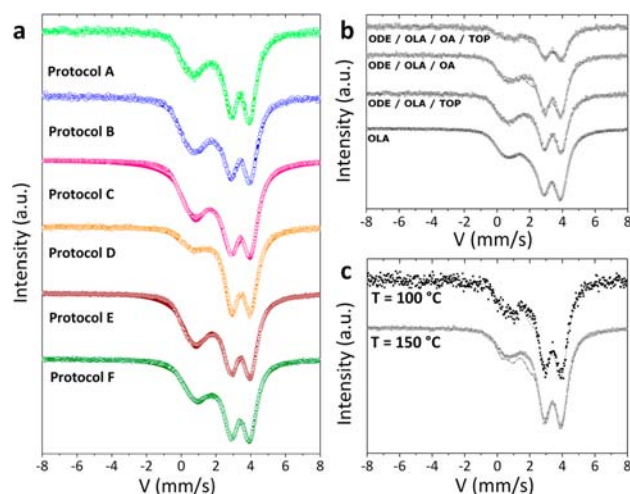


Figure 3. ^{119}Sn -Mössbauer spectra measured at 5K and referred to a BaSnO_3 source of samples prepared (a) using the different synthesis protocols, (b) using protocol A and different ligand combinations, and (c) using protocol A and different reaction temperatures. Dots, experimental spectra; solid lines, fitted spectra.

To understand the mechanism of the $\text{Sn}^{(\text{IV})}$ species formation, we first investigated the influence of NCs surface ligands. Ligands play a key role during NC synthesis, controlling the reaction kinetics and stabilizing the surface of the colloidal particles. By consequence, the chemical nature of the ligands also has a direct impact on the degree of NCs surface oxidation. In this context, interference between different types of ligands could be an issue.⁵⁰ First of all, we found that neither TOP nor OA alone complex tin chloride. To the contrary, a mixture of both compounds conducts to fast complexation, visible by the formation of a transparent solution. We ascribe this behavior to the fact that TOP deprotonates the carboxylic acid function of OA, followed by the complexation of

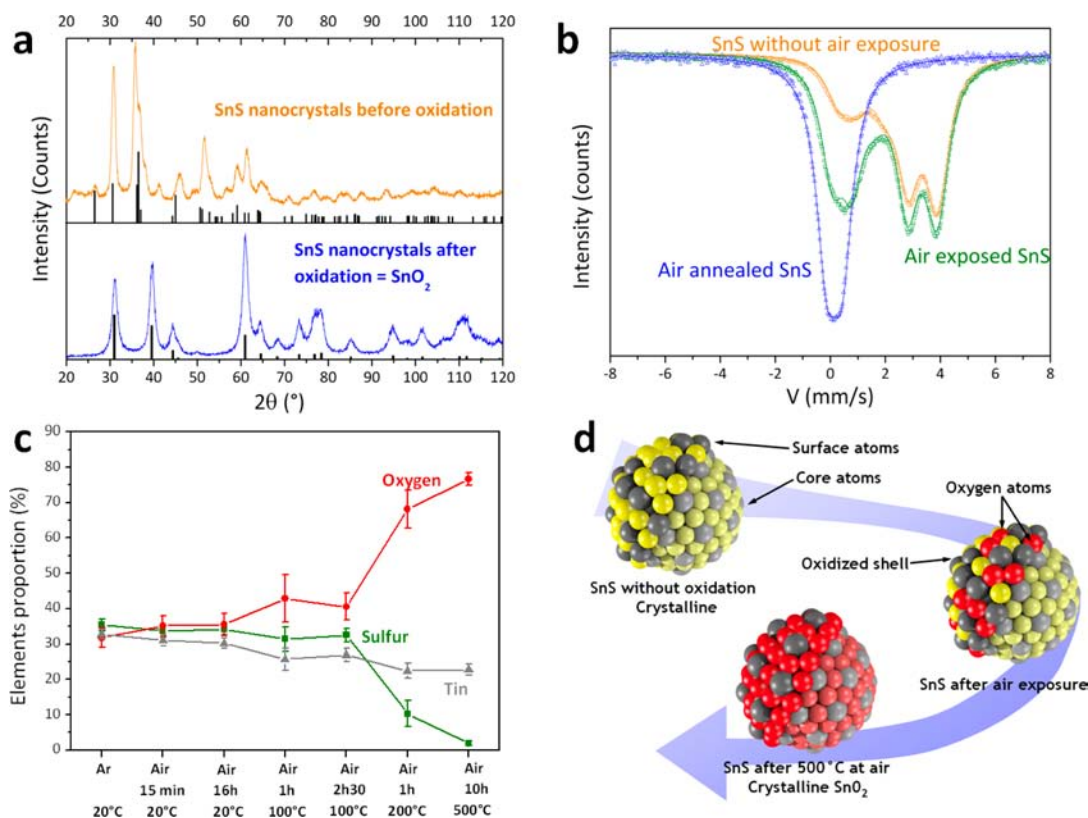


Figure 4. Investigation of the oxidation of SnS NCs. (a) Powder X-ray diffraction (Co K_{α} , $\lambda = 1.789 \text{ \AA}$) with corresponding patterns of the bulk materials (orthorhombic SnS, JCPDS #39–354;⁴⁴ tetragonal cassiterite SnO₂, JCPDS 4–9–8478⁵²); (b) ¹¹⁹Sn Mössbauer spectra recorded at 5 K (green spectrum: air exposure of the sample at room temperature for 5 min, blue spectrum: fully oxidized sample after heating to 500 °C for 10 h); (c) energy dispersive X-ray spectroscopy. (d) Schematic representation of the oxidation mechanism (gray, Sn; yellow, S; red, O).

tin by oleate ions. OLA, on the other hand, complexes tin chloride without the need of other additives. Therefore, in the next step we replaced TOP, OA or both by OLA in order to evaluate the impact of the different ligands on Sn^(II) oxidation. As shown on Figure 3b, no significant changes in the Sn^(II)/Sn^(IV) proportions or in the hyperfine parameters were observed. From these results it is safe to conclude that the surface ligands are not at the origin of the oxidation process. The reaction temperature is an additional parameter of potential influence on surface oxidation. Generally, lower temperatures lead to lower crystallinity of the obtained nanoparticles, and amorphous structures show a higher sensitivity toward oxidation. As can be seen in Figure 3c, carrying out the reaction at 100 °C or at 150 °C does not lead to a significant change in the Mössbauer spectra. In order to study the eventual presence of Sn^(IV) in the used precursor, the latter was analyzed using XRD, tin nuclear magnetic resonance (¹¹⁹SnNMR) and tin Mössbauer spectroscopy (Supporting Information, Figures S3, S4). XRD confirms that the powder corresponds to orthorhombic SnCl₂ (JCPDS #04–007–3801)⁵¹ and ¹¹⁹SnNMR shows no impurity peaks. However, the Mössbauer spectrum of the powder reveals that it contains 2–3% of Sn^(IV) despite its storage and use under inert atmosphere. The low amount of Sn^(IV) in the precursor cannot be alone at the origin of the almost 40% of this species detected in the different samples. This result also confirms the superior sensitivity of Mössbauer spectroscopy as compared to other techniques and in particular to solution NMR spectroscopy.

Finally, we investigated the oxidation process in greater detail by enhancing it willingly through exposure of the NCs to air

combined with heating. As a reference sample, we synthesized SnS NCs following protocol A and carried out all purification steps within a glovebox using completely anhydrous solvents. As shown by XRD (Figure 4a), during exposure to air for 10 h under heating (500 °C), the SnS NCs have been fully transformed to SnO₂ NCs. At the same time, no change in the peak width is observed, indicating that the crystallite size remains the same during oxidation. In the diffractogram of the reference sample (Figure 4a, orange line) and in accordance with the diffractograms in Figure 1b, exclusively the peaks corresponding to SnS in the orthorhombic space group *Pbnm* are observed. The Mössbauer spectra (Figure 4b) show that the Sn^(IV) content of the reference sample accounts for approximately 20%. This value is significantly lower as compared to the samples shown in Figure 3a, which have been purified and stored in air. We attribute the Sn^(IV) species detected in the reference sample (~7 nm SnS NCs) to surface atoms, whose oxidation state depends on their binding to surface ligands, such as oleate molecules. The existence of a ligand induced surface layer of amorphous oxide has also been identified for other material families; in the case of iron oxide or iron platinum nanoparticles it is known as magnetically “dead” layer.^{54,55} Upon air exposure of the reference sample, an increase of the singlet corresponding to Sn^(IV) and the concomitant decrease of the doublet corresponding to Sn^(II) is observed. In the case of the fully oxidized sample, the doublet completely disappeared. The displacement of the isomer shift of the singlet from 0.65 for the reference sample to 0.13 mm s⁻¹ for the oxidized sample can be interpreted as the evolution from a disordered amorphous state to a pure SnO₂ compound

ordered crystalline state. The broadness of the singlet peak suggests an additional peak around 1.2 mm s^{-1} characteristic for the presence of Sn_2S_3 and/or SnS_2 phases.

Monitoring the elemental composition of SnS NCs during the oxidation process using EDS (Figure 4c) strengthens the hypothesis of a substitutional mechanism being at the origin of the transformation. First of all we note that around 30 at.% of oxygen are present in the reference sample, which arise from surface bound oleate molecules, as confirmed by thermogravimetric analyses. At the same time one has to take into account the relatively high uncertainty of the EDS value for oxygen coming from the comparably low signal combined with a low elemental mass. Exposure to air and moderate heating ($100 \text{ }^\circ\text{C}$) result in a small increase of the oxygen content accompanied by the decrease of the sulfur content. After heating to $200 \text{ }^\circ\text{C}$, the massive replacement of sulfur by oxygen is visible, and further heating leads to the formation of SnO_2 NCs. The final O/Sn ratio is slightly higher than expected due to the formation of an oxygen-rich surface upon thermal degradation of the oleate ligands. Figure 4d represents schematically the stepwise oxidation mechanism of SnS NCs.

Surface Passivation with Cd Complexes. To protect SnS NCs against undesired surface oxidation, occurring upon exposure to air as demonstrated in the previous sections, we applied a method of surface passivation by means of cadmium phosphonate complexes. This method has been successfully used by *Sargent's* group for the passivation of PbS NCs and consists of the mixing of the NCs with a Cd-phosphonate complex under gentle heating.¹³ Upon treatment with the Cd complex, the UV-vis absorption spectrum (Figure 5a) of the

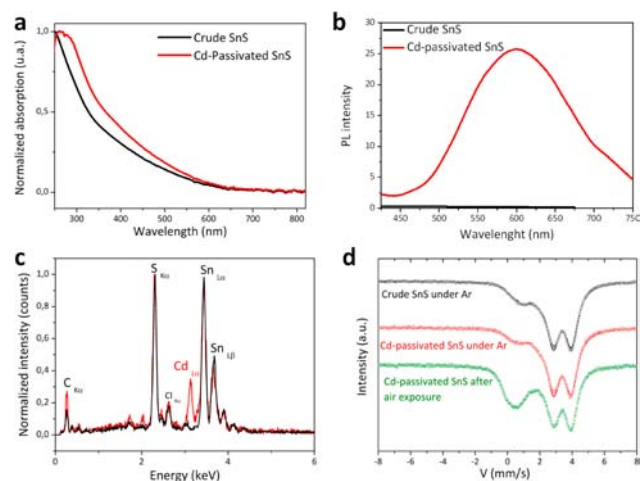


Figure 5. (a) UV-visible absorption spectra, (b) Photoluminescence spectra, (c) EDS measurements, and (d) ^{119}Sn Mössbauer spectra recorded at 5 K of as-synthesized (Protocol D, black) and of Cd-passivated (red) SnS NCs, green spectrum recorded 5 min after exposure to air at ambient temperature.

SnS NCs synthesized using *protocol D* exhibits a slight increase of absorbance in the UV/blue spectral region, as would be expected for a thin layer of CdS (band gap 2.42 eV). The appearance of a broad emission peak centered at approximately 600 nm in PL measurements (Figure 5b) further indicates successful surface passivation removing trap states, which act as nonradiative recombination channels in the case of the untreated sample. Finally, EDS measurements (Figure 5c) showing a Cd content of 12 at.% definitely confirm the

presence of the Cd complex on the surface. As expected, the X-ray diffractogram of the passivated NCs remains unchanged, proving that no cation exchange leading to a ternary compound took place. Mössbauer spectroscopy reveals a slight decrease of the $\text{Sn}^{(\text{IV})}$ peak area of the Cd-passivated NCs with respect to the reference sample of pristine SnS NCs (Figure 5d). However, the hyperfine parameters of the two samples (Supporting Information) yield a fraction of $\text{Sn}^{(\text{II})}$ of $\sim 82\%$ for the Cd-passivated sample compared to $\sim 78\%$ without passivation, that is, a difference which is not significant when taking into account sample-to-sample variations. Furthermore, when measuring the Cd-passivated SnS NCs after air exposure, they show an identical behavior as the pristine SnS NCs, namely a strong increase of the $\text{Sn}^{(\text{IV})}$ peak. Therefore, we can conclude that the surface passivation with Cd-phosphonate complexes is inefficient for preventing SnS NCs from oxidation.

Extension to other tin chalcogenide NCs. For comparative analysis we investigated SnSe and SnTe NCs following reported synthesis procedures.^{29,30} Looking at the UV-vis-NIR absorption spectra of the obtained tin chalcogenide NCs (Figure 6a), SnSe does not seem to exhibit quantum

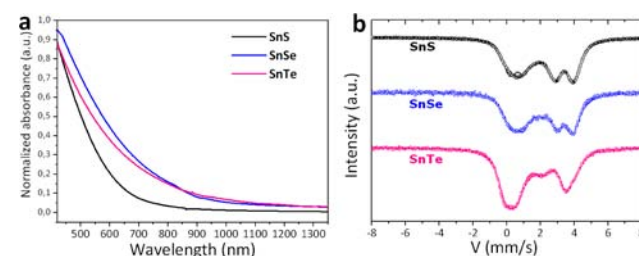


Figure 6. (a) UV-vis-NIR Absorption spectra; (b) ^{119}Sn -Mössbauer spectra recorded at 5 K of SnS, SnSe and SnTe NCs after 10 h of air exposure at room temperature.

confinement with a band gap of 1.4 eV compared to 1.3 eV for the bulk material. On the contrary, SnTe shows a band gap of 1.1 eV , strongly confined with respect to the value of 0.18 eV in the bulk.

It is well known for Cd and Pb chalcogenides that, when going from the sulfides to the heavier homologues of column VI, an increasing tendency for oxidation is observed. Figure 6b compares the ^{119}Sn -Mössbauer spectra obtained with SnS, SnSe and SnTe NCs after air exposure. The first observation is that SnS and SnSe nanocrystals exhibit very similar spectra with $\text{Sn}^{(\text{IV})}:\text{Sn}^{(\text{II})}$ ratios of 42:58 and 43:57. In the case of SnTe NCs, this ratio accounts for 55:45, demonstrating their higher tendency for oxidation. The fitted hyperfine parameters are shown in Supporting Information. The obtained values are summarized in Table 3 and compared to the binding parameters. The bond length increases from SnS to SnTe while the binding strength decreases. Looking at the bulk

Table 3. Bond Distances, Binding Energies, and ^{119}Sn Mössbauer Data of Tin Chalcogenides

	Sn-S	Sn-Se	Sn-Te
Bond distance ⁴⁹	2.65 \AA	2.80 \AA	3.15 \AA
Binding energy ⁵³	464 kJ mol^{-1}	401 kJ mol^{-1}	360 kJ mol^{-1}
Isomer shift of $\text{Sn}^{(\text{II})}$ (literature) ⁴⁹	3.4 mm s^{-1}	3.4 mm s^{-1}	3.5 mm s^{-1}
Isomer shift of $\text{Sn}^{(\text{II})}$ (this study)	3.3 mm s^{-1}	3.4 mm s^{-1}	3.7 mm s^{-1}

materials, Lippens reported increasing isomer shift values with increasing bond lengths.⁴⁹ In our case, this trend is accompanied by a 0.4 mm.s⁻¹ shift of the IS value corresponding to Sn^(IV) when going from SnS to SnTe. To sum up, nanocrystalline tin chalcogenides are air sensitive and exhibit significant surface oxidation even at room temperature. The degree of oxidation can precisely be monitored by ¹¹⁹Sn Mössbauer spectroscopy. The air-sensitivity increases for the heavier homologue SnTe, while SnS and SnSe present a lower fragility due to the comparably strong bonds between tin and sulfur or selenium, respectively.

CONCLUSION

¹¹⁹Sn Mössbauer spectroscopy has been used to investigate the Sn atoms oxidation state in tin chalcogenide NCs. Independent of the tin and sulfur precursors, combination of surface ligands and reaction temperature, "SnS" NCs exhibit a Sn^(IV)/Sn^(II) ratio of around 40:60 after exposure to air, clearly showing their high sensitivity toward oxidation. They can be completely transformed to SnO₂ NCs by simple thermal annealing. The surface oxide layer presumably prevents from NCs' sintering during this heating step. Passivation with Cd phosphonate, which has been proven efficient for increasing the stability of PbS NCs does not reduce the air sensitivity of SnS NCs. Mössbauer spectroscopy also reveals that SnSe NCs show very similar behavior as SnS NCs, while SnTe NCs are more prone to oxidation. This work emphasizes that for the successful integration into (opto-)electronic applications, tin chalcogenide NCs need to be handled, purified and processed under inert atmosphere. Alternatively, progress in the surface engineering of tin chalcogenide NCs could improve their air-stability.

ASSOCIATED CONTENT

Supporting Information

EDS measurements, Mössbauer fitting parameters, SEM images, and characterization of the used tin chloride precursor by ⁵¹V NMR, Mössbauer spectroscopy and XRD. This material is available free of charge via the Internet at <http://pubs.acs.org>.

AUTHOR INFORMATION

Corresponding Author

*peter.reiss@cea.fr

Notes

The authors declare no competing financial interest.

ACKNOWLEDGMENTS

This research was supported by the Micro-Nano and Energy research clusters of the Region Rhône-Alpes. We thank Dr. Angela Fiore, Dr. Stéphanie Pouget, Dr. Sudarsan Tamang, Dr. Frédéric Chandezon and Axel Maurice for helpful discussions and Pierre-Alain Bayle for NMR measurements. Pierre Delcroix from Institut Jean Lamour is acknowledged for help with ¹¹⁹Sn Mössbauer Spectroscopy.

REFERENCES

- (1) Talapin, D. V.; Lee, J.-S.; Kovalenko, M. V.; Shevchenko, E. V. *Chem. Rev.* **2010**, *110*, 389–458.
- (2) Lee, J.-S.; Kovalenko, M. V.; Huang, J.; Chung, D. S.; Talapin, D. V. *Nat. Nanotechnol.* **2011**, *6*, 348–352.
- (3) Talapin, D. V.; Murray, C. B. *Science* **2005**, *310* (5745), 86–89.
- (4) Shimoda, T.; Matsuki, Y.; Furusawa, M.; Aoki, T.; Yudasaka, I.; Tanaka, H.; Iwasawa, H.; Wang, D.; Miyasaka, M.; Takeuchi, Y. *Nature* **2006**, *440*, 783–786.

- (5) Urban, J. J.; Talapin, D. V.; Shevchenko, E. V.; Kagan, C. R.; Murray, C. B. *Nat. Mater.* **2007**, *6*, 115–121.
- (6) Mitzi, D. B.; Copel, M.; Chey, S. J. *Adv. Mater.* **2005**, *17*, 1285–1289.
- (7) Ong, B. S.; Li, C.; Li, Y.; Wu, Y.; Loutfy, R. J. *Am. Chem. Soc.* **2007**, *129*, 2750–2751.
- (8) Luther, J. M.; Law, M.; Beard, M. C.; Song, Q.; Reese, M. O.; Ellingson, R. J.; Nozik, A. J. *Nano Lett.* **2008**, *8*, 3488–3492.
- (9) Dayal, S.; Kopidakis, N.; Olson, D. C.; Ginley, D. S.; Rumbles, G. *Nano Lett.* **2010**, *10*, 239–242.
- (10) Kamat, P. V.; Tvrđy, K.; Baker, D. R.; Radich, J. G. *Chem. Rev.* **2010**, *110*, 6664–6688.
- (11) Gao, J.; Luther, J. M.; Semonin, O. E.; Ellingson, R. J.; Nozik, A. J.; Beard, M. C. *Nano Lett.* **2011**, *11*, 1002–1008.
- (12) Wang, X.; Koleilat, G. I.; Tang, J.; Liu, H.; Kramer, I. J.; Debnath, R.; Brzozowski, L.; Barkhouse, D. A. R.; Levina, L.; Hoogland, S.; Sargent, E. H. *Nat. Photon.* **2011**, *5*, 480–484.
- (13) Tang, J.; Kemp, K. W.; Hoogland, S.; Jeong, K. S.; Liu, H.; Levina, L.; Furukawa, M.; Wang, X.; Debnath, R.; Cha, D.; Chou, K. W.; Fischer, A.; Amassian, A.; Asbury, J. B.; Sargent, E. H. *Nat. Mater.* **2011**, *10*, 765–771.
- (14) Debnath, R.; Bakr, O.; Sargent, E. H. *Ener. Environ. Sci.* **2011**, *4*, 4870–4881.
- (15) Choi, H.; Nicolaescu, R.; Paek, S.; Ko, J.; Kamat, P. V. *ACS Nano* **2011**, *5*, 9238–9245.
- (16) Hetsch, F.; Xu, X.; Wang, H.; Kershaw, S. V.; Rogach, A. L. *J. Phys. Chem. Lett.* **2011**, *2*, 1879–1887.
- (17) Panthani, M. G.; Akhavan, V.; Goodfellow, B.; Schmidtke, J. P.; Dunn, L.; Dodabalapur, A.; Barbara, P. F.; Korgel, B. A. *J. Am. Chem. Soc.* **2008**, *130*, 16770–16777.
- (18) Steinhausen, C.; Panthani, M. G.; Akhavan, V.; Goodfellow, B.; Koo, B.; Korgel, B. A. *J. Am. Chem. Soc.* **2009**, *131*, 12554–12555.
- (19) Shavel, A.; Arbiol, J.; Cabot, A. *J. Am. Chem. Soc.* **2010**, *132*, 4514–4515.
- (20) de Kergommeaux, A.; Fiore, A.; Bruyant, N.; Chandezon, F.; Reiss, P.; Pron, A.; de Bettignies, R.; Faure-Vincent, J. *Sol. Ener. Mat. Sol. Cells* **2011**, *95*, S39–S43.
- (21) Puthusser, J.; Seefeld, S.; Berry, N.; Gibbs, M.; Law, M. *J. Am. Chem. Soc.* **2011**, *133*, 716–719.
- (22) Bi, Y.; Yuan, Y.; Exstrom, C. L.; Darveau, S. A.; Huang, J. *Nano Lett.* **2011**, *11*, 4953–4957.
- (23) Li, W.; Döblinger, M.; Vaneski, A.; Rogach, A. L.; Jäckel, F.; Feldmann, J. *J. Mater. Chem.* **2011**, *21*, 17946–17952.
- (24) Wu, Y.; Wadia, C.; Ma, W.; Sadtler, B.; Alivisatos, A. P. *Nano Lett.* **2008**, *8*, 2345–2350.
- (25) Kriegel, I.; Jiang, C.; Rodríguez-Fernández, J.; Schaller, R. D.; Talapin, D. V.; da Como, E.; Feldmann, J. *J. Am. Chem. Soc.* **2012**, *134*, 1583–1590.
- (26) Hickey, S. G.; Waurisch, C.; Rellinghaus, B.; Eychmüller, A. *J. Am. Chem. Soc.* **2008**, *130*, 14978–14980.
- (27) Liu, H.; Liu, Y.; Wang, Z.; He, P. *Nanotechnology* **2010**, *21*, 105707.
- (28) Baumgardner, W. J.; Choi, J. J.; Lim, Y.-F.; Hanrath, T. *J. Am. Chem. Soc.* **2010**, *132*, 9519–9521.
- (29) Kovalenko, M. V.; Heiss, W.; Shevchenko, E. V.; Lee, J.-S.; Schwinghammer, H.; Alivisatos, A. P.; Talapin, D. V. *J. Am. Chem. Soc.* **2007**, *129*, 11354–11355.
- (30) Kovalenko, M. V.; Scheele, M.; Talapin, D. V. *Science* **2009**, *324*, 1417–1420.
- (31) Kovalenko, M. V.; Bodnarchuk, M. I.; Zaumseil, J.; Lee, J.-S.; Talapin, D. V. *J. Am. Chem. Soc.* **2010**, *132*, 10085–10092.
- (32) Nag, A.; Kovalenko, M. V.; Lee, J.-S.; Liu, W.; Spokoynny, B.; Talapin, D. V. *J. Am. Chem. Soc.* **2011**, *133*, 10612–10620.
- (33) Zhang, H.; Hu, B.; Sun, L.; Hovden, R.; Wise, F. W.; Muller, D. A.; Robinson, R. D. *Nano Lett.* **2011**, *11*, 5356–5361.
- (34) Kovalenko, M. V.; Schaller, R. D.; Jarzab, D.; Loi, M. A.; Talapin, D. V. *J. Am. Chem. Soc.* **2012**, *134*, 2457–2460.

- (35) Kinder, E.; Moroz, P.; Diederich, G.; Johnson, A.; Kirsanova, M.; Nemchinov, A.; O'Connor, T.; Roth, D.; Zamkov, M. *J. Am. Chem. Soc.* **2011**, *133*, 20488–20499.
- (36) Nayral, C.; Viala, E.; Fau, P.; Senocq, F.; Jumas, J.-C.; Maisonnat, A.; Chaudret, B. *Chem.—Eur. J.* **2000**, *6*, 4082–4090.
- (37) Kida, T.; Doi, T.; Shimanoe, K. *Chem. Mater.* **2010**, *22*, 2662–2667.
- (38) Nayral, C.; Ould-Ely, T.; Maisonnat, A.; Chaudret, B.; Fau, P.; Lescouzères, L.; Peyre-Lavigne, A. *Adv. Mater.* **1999**, *11*, 61–63.
- (39) Nayral, C.; Viala, E.; Collière, V.; Fau, P.; Senocq, F.; Maisonnat, A.; Chaudret, B. *Appl. Surf. Sci.* **2000**, *164*, 219–226.
- (40) Cabot, A.; Arbiol, J.; Morante, J. R.; Weimar, U.; Bârsan, N.; Göpel, W. *Sens. Actuat. B* **2000**, *70*, 87–100.
- (41) Cabot, A.; Diéguez, A.; Romano-Rodríguez, A.; Morante, J. R.; Bârsan, N. *Sens. Actuat. B* **2001**, *79*, 98–106.
- (42) Fujihara, S.; Maeda, T.; Ohgi, H.; Hosono, E.; Imai, H.; Kim, S.-H. *Langmuir* **2004**, *20*, 6476–6481.
- (43) Wang, H.; Fu, F.; Zhang, F.; Wang, H.-E.; Kershaw, S. V.; Xu, J.; Sun, S.-G.; Rogach, A. L. *J. Mater. Chem.* **2012**, *22*, 2140–2148.
- (44) Sugaki, A.; Kitakaze, A.; Kitazawa, H. *Science Reports of the Tohoku Imperial University; 3rd Series* **1985**, *16*, 199–211.
- (45) Nassary, M. M. *J. All. Comp.* **2005**, *398*, 21–25.
- (46) Mazet, T.; Ihou-Mouko, H.; Malaman, B. *Appl. Phys. Lett.* **2006**, *89*, 022503.
- (47) Venturini, G.; Lemoine, P.; Malaman, B. *J. All. Comp.* **2011**, *509*, 4660–4669.
- (48) Mazet, T.; Recour, Q.; Malaman, B. *Phys. Rev. B* **2010**, *81*, 174427.
- (49) Lippens, P. E. *Phys. Rev. B* **1999**, *60*, 4576–4586.
- (50) Protière, M.; Reiss, P. *Chem. Commun.* **2007**, 2417–2419.
- (51) Van den Berg, J. M. *Acta Crystallogr.* **1961**, *14*, 1002–1003.
- (52) Gracia, L.; Beltran, A.; Andres, J. *J. Phys. Chem. B* **2007**, *111*, 6479–6485.
- (53) D. R. Lide, Ed. *CRC Handbook of Chemistry and Physics*, 89th ed; CRC Press: Boca Raton, FL.
- (54) Stahl, B.; Gajbhiye, N. S.; Wilde, G.; Kramer, D.; Ellrich, J.; Ghafari, M.; Hahn, H.; Gleiter, H.; Weissmüller, J.; Würschum, R.; Schlossmacher, P. *Adv. Mater.* **2002**, *14*, 24–27.
- (55) Delalande, M.; Marcoux, P. R.; Reiss, P.; Samson, Y. *J. Mater. Chem.* **2007**, *17*, 1579–1588.